Published in final edited form as:
J Comp Neurol. 2008 September 10; 510(2): 221–236. doi:10.1002/cne.21795.

The Spatial Distribution of Glutamatergic Inputs to Dendrites of Retinal Ganglion Cells

Tatjana C. Jakobs[*], **Amane Koizumi**[*], and **Richard H. Masland**
Massachusetts General Hospital, Harvard Medical School, Boston, MA 02114

Abstract

The spatial pattern of excitatory glutamatergic input was visualized in a large series of ganglion cells of the rabbit retina, using particle-mediated gene transfer of an expression plasmid for PSD95-GFP. PSD95-GFP was confirmed as a marker of excitatory input by co-localization with synaptic ribbons (RIBEYE and kinesin II) and glutamate receptor subunits. Despite wide variation in the size, morphology, and functional complexity of the cells, the distribution of excitatory synaptic inputs followed a single set of rules: (1) The linear density of synaptic inputs (PSD95 sites / linear μm) varied surprisingly little and showed little specialization within the arbor. (2) The total density of excitatory inputs across individual arbors peaked in a ring-shaped region surrounding the soma. This is in accord with high-resolution maps of receptive field sensitivity in the rabbit. (3) The areal density scaled inversely with the total area of the dendritic arbor, so that narrow dendritic arbors receive more synapses per unit area than large ones. To achieve sensitivity comparable to that of large cells, those that report upon a small region of visual space may need to receive a denser synaptic input from within that space.

Keywords

retinal ganglion cells; PSD95; excitatory synaptic input; synapse distribution; organotypic retina culture

Introduction

This study asks the question: do distinct spatial patterns of excitatory synaptic input characterize the functionally distinct types of retinal neurons? In the retina of the rabbit, which has been especially well studied, there are ~ 12 distinct types of retinal ganglion cells. These are separable on morphological criteria, and for many a distinct physiology has been established. For example, one cell type responds to the direction of movement of fairly large images; while another (the " local edge detector") responds to any direction of movement but within a far smaller area of the retina, and within that area only to small, solitary objects (Levick, 1967; Caldwell and Daw, 1978; Amthor et al., 1989a; Amthor et al., 1989b; Roska and Werblin, 2001; Rockhill et al., 2002; Roska et al., 2006; van Wyk et al., 2006).

Much evidence from elsewhere in the nervous system suggested that synapses would be differentially located around the dendritic arbors (Gulyas et al., 1999; Megias et al., 2001; García-López et al., 2006). In CA1 hippocampal neurons, for example, the density of excitatory inputs ranged from 7.12 synapses/ linear μm in the thick distal dendrites of the stratum radiatum to 0.03 in the proximal ones. The ratio of inhibitory input to excitatory

Correspondence: Richard Masland Massachusets General Hospital, Thier 429 50 Blossom Street Boston, MA 02114 Tel: (+1) 617 726 3888 richard_masland@hms.harvard.edu.
[*]The first two authors contributed equally to this work.

input in the same structures ranged from 2% to 98%, in accord with the principle that inhibitory inputs are often positioned for on-path shunting of excitatory currents traveling toward the soma (Megias et al., 2001). Thus, there are anisotropies of both number and kind of synapses across the dendritic arbors of these cells.

In contrast, existing studies of some types of retinal ganglion cells suggest a less specialized distribution. Serial section electron microscopy has been carried out on midget cells in the macaque monkey (Calkins and Sterling, 1996; Klug et al., 2003); parasol cells in the macaque monkey (Jacoby et al., 1996; Marshak et al., 2002); blue — ON cells in the macaque (Calkins et al., 1998); alpha cells in the cat (Freed and Sterling, 1988); and beta cells in the cat (Sterling, 1983; McGuire et al., 1986; Cohen and Sterling, 1991). In addition, high resolution light microscopy has been used to localize both excitatory and inhibitory receptors on midget, parasol, and blue-ON cells, and local edge detectors in the marmoset monkey (Lin et al., 2000; Macri et al., 2000; Lin et al., 2002; Jusuf et al., 2006) and the guinea pig (Xu et al., 2008). A previous study of the ON —Off direction selective cell in the rabbit localized bipolar input and GABA receptors (Jeon et al., 2002). These different studies all used slightly different techniques. Furthermore, the receptive fields of many cell types studied were relatively simple. Here, we sought to survey a spectrum of physiological cell types, under uniform technical conditions; to include cells with both simple and complex receptive fields; and to create a larger database of cells than has heretofore been possible. We wanted to see, especially for the larger and more physiologically complex cells, whether there was a correlation between synaptic patterns and the distinct physiological tasks of individual types of retinal ganglion cells.

To address this question, we needed a way to visualize synaptic inputs upon the cell. The synapses of retinal ganglion cells fall directly upon the dendritic shafts, so that spines cannot be counted. Electron microscopic reconstruction would have been prohibitively slow. An alternative is to use high resolution light microscopy to identify immunostained components of synapses (Koulen et al., 1996; Grünert and Ghosh, 1999; Lin et al., 2000; Jeon et al., 2002; Li et al., 2002; Xu et al., 2008). In skilled hands, this is a viable strategy, but its technical demands are great. When dendrites of a cell are embedded in a dense neuropil, the neuropil presents a three dimensional array of fluorescent puncta representing the synapse component under study. A marked dendrite threads its way through this array and the problem is to know which puncta belong to the marked dendrite and which to dendrites of other cells. While spatial algorithms can aid this decision, it challenges the limits of light microscopy and requires that all components of the images be of great technical precision.

We therefore used a different approach, in which the synapse marker was expressed only in the single cell under investigation. In that case, synaptic puncta belong, by definition, to the cell of interest. A platform for this type of experiment was provided by a newly developed system for short term organ culture of the intact retina, which allowed sufficient time for gene expression in adult retinas (Koizumi et al., 2007). Fluorescently labeled synapse markers were introduced by particle mediated transfer of the appropriate plasmids (Lo et al., 1994). Following the precedent of Morgan et al. (Morgan et al., 2008), we concentrated especially on PSD95, a protein that links most types of glutamate receptors to the cytoskeleton (Wong et al., 1991; Marrs et al., 2001; Ebihara et al., 2003; Sanchez et al., 2006; Zhang and Diamond, 2006).

We found that the anisotropies expected from projection neurons elsewhere in the nervous system do not exist in retinal ganglion cells: as for the simpler cells previously studied, excitatory synapses were evenly distributed along almost all of the dendrites, and this was true for all of the diverse cell types that we studied -- large cells and small ones, complex physiologies and simple ones, cells stratified at all levels of the inner plexiform layer. We

quantified the distributions of synapses on the cells. A few general rules seemed to govern all cell types.

Materials and Methods

Organotypic culture of adult rabbit retina

Eight New Zealand white rabbits of either sex aged 7-10 weeks were enucleated under deep anesthesia and euthanized according to a protocol approved by the Subcommittee on Research Animal Care of the Massachusetts General Hospital. Preparation and incubation of the retinas for 4 days was described in detail elsewhere (Koizumi et al., 2007). In brief, ~ 1 cm^2 pieces of retina were mounted on a 0.4 μm Millicell filter (Millipore), placed at the interphase between Ames' medium and air/5% CO_2 and incubated with agitation in a humidified incubator at 37 °C. The ganglion cell side of the retina was facing up, and all subsequent manipulations were performed on the filters.

Preparation of Plasmids and Gene-Gun Bullets

The expression plasmid pPSD95-GFP was a kind gift of Dr. Morgan Sheng (MIT, Cambridge, MA). It allows the expression of a fusion protein of full-length PSD95 and GFP so that the C-terminus of PSD95 is linked via 3 glycine residues (introduced in the cloning process) to the N-terminus of GFP (for details see Arnold and Clapham, 1999). The plasmid pHcRed-N1 was purchased from Clontech (Palo Alto, CA). Retinal ganglion cells were transfected via particle-mediated gene transfer using the Helios Gene Gun System (BioRad, Hercules, CA). The ratio of DNA to the gold microcarriers (mean diameter 1.6 μm) was 1.5 μg plasmid / 1 mg gold. Ganglion cells were transfected by propelling the gold bullets into the tissue with pressurized helium at 90-120 psi. Generally, 30-100 ganglion cells (and displaced amacrine cells) were labeled per cm^2 of retina.

Patch-Clamp recordings from ganglion cells of incubated retina

To test the integrity of incubated retinas, whole-cell patch-clamp recordings were carried out from some tissues. The recording techniques were conventional (Koizumi et al., 2004; Koizumi et al., 2007). Patch pipettes 1-2 μm tip diameter had a resistance of approximately 10-15 MΩ when filled with the pipette solution (in mM): 87 K-gluconate, 7 KCl, 5 HEPES, 0.4 CaCl2, 0.4 MgCl2, 5 EGTA and 2 ATP-Na2 (pH adjusted to 7.4 with KOH). Signals were sampled at 10 kHz with DigiData 1322A interface-type and pCLAMP8 software (Axon Instruments). The liquid junction potential was measured as 17 mV (Vm = Vp — 17 mV) and corrected after recordings. Subsequent analysis was done by custom-made procedures in Igor Pro (WaveMetrics, Lake Oswego, OR, USA). Photo-stimuli were generated on a calibrated CRT monitor (Dell-P780, SONY, Japan) using Visionworks (Vision Research Graphics, Durham, NH) and were reflected upward by a mirror positioned underneath the recording chamber. A microscope objective (Olympus Optical, Tokyo, Japan; 20x, N.A. 0.4) focused the stimulus on the retina.

Identification of ganglion cell types

For this study we focused upon a series of six types of ganglion cell. They span extremes in morphology and physiological behavior. There is agreement from many studies by independent laboratories on their physiology and its morphological concomitant (Amthor et al., 1989a; Amthor et al., 1989b; He and Masland, 1998; Roska and Werblin, 2001; Rockhill et al., 2002; Roska et al., 2006).

The *Local Edge Detector (LED)* has the smallest receptive field of any ganglion cell in the rabbit, often < 150 μm in diameter. The cells are virtually unresponsive to diffuse light or to patterned stimuli that cover the whole receptive field. They respond best to contrast that is

restricted to the center of the receptive field, without traversing the receptive field's borders. In keeping with its small receptive field, the LED is the smallest ganglion cell in the rabbit retina, with a dendritic arbor about 150-200 μm in diameter (Rockhill et al., 2002). The cells are monostratified relatively narrowly at 40-50 % of the inner plexiform layer, receiving input at ON- and OFF. Their dendritic arbors contain 4-7 main branches and numerous small twigs (Levick, 1967; Amthor et al., 1989a; Zeck et al., 2005; Roska et al., 2006).

A bistratified cell, G3 in the nomenclature of Rockhill et al., may be the Blue — ON , although this identification has not been confirmed physiologically. It is the only one in this series whose physiological identity has not been directly confirmed by recording with subsequent anatomical identification in the rabbit. In other mammals, these cells have a spatially simple (round) receptive field. Its distinguishing feature is that the cell responds by excitation when short wavelengths fall upon the receptive field and is inhibited by long wavelengths. A Blue ON cell has been recorded in the rabbit (Caldwell and Daw, 1978) and the bistratified cell identified here has the morphology of the blue ON cell in other species (Dacey, 1993; Calkins et al., 1998; Masland, 2001).

The cell termed G5 shows a transient OFF response (Roska et al., 2006). Its dendritic arbor is ~ 250 μm in diameter, and stratified at 20 % of the inner plexiform layer. It is distinguished by its exceptionally narrow stratification within the ipl (see Figure 2 F). This cell may correspond to the parasol cell of (Roska et al., 2006).

The *ON — OFF directionally selective cell* (G7 in Rockhill et al., 2002) gives ON - OFF responses to flashed stimuli and gives directional responses to a wide range of speeds of stimulus movement. It is a large cell with a distinctive bistratified dendritic arbor and has been the focus of a great many anatomical and physiological studies (Barlow and Levick, 1965; Amthor et al., 1984; Yang and Masland, 1992; Roska and Werblin, 2001; Fried et al., 2002; Roska et al., 2006).

The less frequent *ON DS cell* (G10 in Rockhill et al., 2002) gives ON responses to flashed stimuli and responds to very slow stimulus movement. Its ON directionally selective characteristics have been demonstrated by recording (Oyster et al., 1980; Amthor et al., 1989a; He and Masland, 1998).

The *Brisk-Transient cell*, (G11 in Rockhill et al., 2002) which has ON and OFF variants, has a large receptive field and non-linear electrophysiological responses similar to those of the Y (alpha) cell of the cat (Cleland and Levick, 1974; Caldwell and Daw, 1978; Amthor et al., 1989b; Roska et al., 2006). It responds to the onset or offset of light with a brief, high frequency burst of spikes. This is the largest ganglion cell in the rabbit, with a dendritic arbor that can reach 1 mm in diameter (Peichl et al., 1987).

Immunostaining, Image Acquisition, and Analysis

Four days after transfection with expression plasmids for PSD95-GFP the retinas were harvested and fixed for 30 min in 4% paraformaldehyde. Some retinas were left on the Millicell filter and used immediately for immunostaining as whole-mounts; 56 ganglion cells were counterstained for Kif3a or RIBEYE, 3 for GluR2/3, and 5 for GABAA receptor. In this case the tissue was incubated with the primary antibodies at 4 °C for one week. A rabbit polyclonal antibody against the carboxyterminal peptide (EGYNVYGIESVKI) from rat glutamate receptors GluR2/3 was obtained from Chemicon (Temecula, CA, catalog # AB1506, lot # 22061130, the antibody does not distinguish between isoforms GluR2 and GluR3) and used at 4 μg/ml. The antibody against GluR2/3 was tested for specificity in Western blots, where it labeled a single band of ~110 kD in mouse brain extracts that was absent from liver extracts, in agreement with the known expression of this protein in nervous

tissue. The mouse monoclonal anti-GABA A receptor α1-chain (Chemicon, catalog # MAB339, lot # 19050429, Clone BD24, raised against purified GABA receptor from bovine brain) was used at 4 μg/ml. This antibody was shown to recognize a 51 kD band in Western blots of hippocampal tissue (Rissman et al., 2003). When tested in vertical sections, it gave a punctate labeling throughout the IPL, which is consistent with the pattern observed for this subunit in earlier studies (Sassoè-Pognetto et al., 1995). The rabbit polyclonal antibody against the C-terminal domain (amino acids 361-445) of CtBP2 (RIBEYE) was purchased from BD Biosciences (San Jose, CA, catalog # 612044, lot # 39302) and used at 2 μg/ml. The synaptic ribbon component RIBEYE has been shown to be a fusion protein form a unique A domain and a B domain identical to the transcriptional repressor CtBP2 (Schmitz et al., 2000). The anti-CtBP2 antibody recognizes RIBEYE in retinal extract as double bands of ~120 and ~110 kD, and it also labels synaptic ribbons in immuno-electron microscopy (tom Dieck et al., 2005). The mouse monoclonal antibody against the synaptic ribbon component Kif3a (kinesin II, generated against kinesin II purified from sea urchin eggs) was purchased from Covance (Richmond, CA, catalog # MMS-198P, lot # 147333001) and used at 20 μg/ml. The anti-Kif3a antibody has been characterized in earlier studies where it was found to recognize a close doublet of ~80 kD bands in rat retina extract; in vertical sections, it labels punctate structures in the IPL and larger, often horseshoe-shaped profiles in the OPL, consistent with synaptic ribbon labeling whereas no such labeling is seen with pre-immune serum. This antibody has also been used to label synaptic ribbons in immuno-electron microscopy (Muresan et al., 1999). Both anti-Kif3a and anti-RIBEYE have been used to identify synaptic ribbons in the retinas of several mammalian species, including rabbit (Hildebrand and Soriano, 2002; Jeon et al., 2002; Hirano et al., 2007; Xu et al., 2008). All antibodies were tested on vertical agarose sections (50 μm) of rabbit retina before use in co-localization studies.

Immunostaining was visualized using secondary antibodies coupled to rhodamine. The single immunolabeling for CtBP2 in Figure 6 was revealed with secondary antibodies coupled to FITC (all secondary antibodies were from Jackson Immunoresearch Laboratories, West Grove, PA). Occasionally, nuclei were counterstained using TOPRO3 (Invitrogen) or DAPI (Sigma). The tissue was mounted in Vectashield (Vector Laboratories, Burlingame, CA) and imaged the day after mounting. Image acquisition was performed on a BioRad Radiance confocal system equipped with krypton/argon and CO_2 lasers and mounted on a Zeiss Axioscope II.

For the imaging of PSD95-GFP puncta on individual ganglion cells, through-focus z-stacks were taken at 63× from the INL/IPL border to the IPL/GCL border. The step size in the z-dimension was matched with the nominal x/y pixel resolution (usually 0.4 μm). For small ganglion cells close to the visual streak, one image stack usually sufficed. For large cells (such as Brisk Transient or peripheral DS cells), several image stacks from nearby regions were taken at the same magnification and montaged using Photoshop 7.0 (Adobe Systems, Inc., San Jose, CA). No other digital image processing was carried out on these image stacks.

After immunohistochemistry a survey z-stack was taken at low magnification and individual dendrites were chosen for imaging at high resolution (63x objective with optical zoom settings of 2-4 fold). The degree of association of structures labeled in two channels (for example, PSD95-GFP puncta in green, and synaptic ribbons stained with anti-Kif 3a or anti-RIBEYE in magenta) was analyzed by a method similar to the one described by Li et al (Li et al., 2002) using Matlab (The Mathworks, Lowell, MA). The total number of partial dendritic arbors analyzed was 14 (6 for PSD95 and Kif3a or RIBEYE, 3 for PSD95 and GluR2/3, and 5 for PSD95 and GABAA receptor).

Synaptic ribbons were counted on optical sections through the IPL from the border of the INL (0% depth) the border of the GCL (100% depth). The images were median filtered, thresholded, and the number of individual ribbons was counted with a user-written Matlab routine.

For quantitative analysis of dendritic structure, the Neurolucida software package (Microbrightfield, Williston, VT) was used to trace individual ganglion cells from confocal image stacks. The dendritic tree was traced in 3 dimensions by stepping up and down through the image stack so that the dendrite stayed in focus. This is possible because in addition to the bright PSD95-GFP puncta a dim background labeling, presumably due to PSD95-GFP in transit, is discernable. The localization of PSD95 puncta was recorded by placing markers on the digitized cell drawing, also in Neurolucida.

Some previous workers have reported the nominal density of synaptic contacts using as a baseline the apparent area of dendritic membrane in the vicinity, i.e. puncta / μm^2. For some purposes, such as biophysical modeling, this may in principle have advantages. However, where the sampling of the retinal surface (i.e. the mosaic of the cell's inputs and outputs) is concerned, the dendritic area at different points is only a confounding variable. Furthermore, this measurement is virtually impossible to make by light microscopy with precision: for very thin objects, such as dendrites, there is major confounding of thickness and brightness. This is especially dangerous since many labeling methods give non-uniform brightness to different parts of the dendritic tree. To make things even worse, the estimation of dendritic "area" depends on the square of the quantity actually measured, which is the dendritic radius. This amplifies the already large errors of measurement. By contrast, measuring dendritic length is easy and reliable. It is a much more robust quantity and was used as a base of reference here.

Analysis of the distribution of PSD95-GFP puncta

We calculated one-dimensional and two dimensional density of PSD95-GFP puncta in MatLab from NeuroLucida traces as follows: The one dimensional density of PSD95-GFP puncta on the dendrites was calculated as number of puncta / dendrite length (μm) (Table 1 and Figure 5). Intervals between pairs of adjacent puncta were also measured (Table 1). The two dimensional density of PSD95-GFP within the dendritic field was calculated as number of puncta / area (mm^2). The areal density as a function of distance from the soma of the cells is shown in Figure 8. The dendritic field of the cells was determined by the convex hull function in MatLab and the equivalent diameter of the dendritic field was calculated from the measured areas (Table 1).

Results

Organotypic culture and gene expression

Figure 1 A&B shows the intact dendritic arbors of ganglion cells transfected with EGFP-F, a cell membrane-targeted variant of the fluorescent protein. The neurons retain their characteristic size, stratification, and branching pattern for at least 6 days. Only at the end of that time were there hints of rearrangement, notably retraction of the severed axon and occasionally of the terminal tips of the dendrites. As a sensitive test of the tissue's viability, we conducted whole-cell patch-clamp recordings from ganglion cells in retinas incubated for up to 6 days. The cells had normal resting potentials and generated trains of action potentials in response to current injection. Retinas isolated under dim light and maintained in the dark for up to 4 days showed normal morphology (Figure 1 C) and unequivocal responses to light in patch recordings (Figure 1 D). After 6 days in culture, recording of light responses became less reliable (this is perhaps because of lack of visual pigment regeneration in the

absence of the pigment epithelium). Accordingly, the experiments described here allowed 4 days or less for gene expression.

The expression of PSD95-GFP indicates the locations of excitatory synapses upon retinal ganglion cells

Retinal ganglion cells were gene gunned with a plasmid encoding PSD95-GFP. The resulting images contained brightly fluorescent puncta distributed around the dendritic arbors. A much fainter background labeling, presumably arising from PSD95-GFP in transit was also observed. This is in agreement with observations in earlier studies (Ebihara et al., 2003) and helps to identify the dendrite itself (see Figure 2A). The pattern of labeling was consistent between cells. The total number and densities of PSD95-GFP puncta (Table 1) are similar to estimates of excitatory synapses arrived at by other researchers using different methods (McGuire et al., 1986; Freed and Sterling, 1988; Cohen and Sterling, 1991; Weber et al., 1991; Weber and Stanford, 1994; Jacoby et al., 1996; Ghosh and Grünert, 1999; Owczarzak and Pourcho, 1999; Jacoby et al., 2000; Lin et al., 2002; Dacheux et al., 2003; Famiglietti, 2005). PSD95-GFP were virtually absent from primary dendrites and those dendrites (Figure 2 A&B) that traverse the IPL vertically from the soma, or that connect ON- and OFF arbors of bistratified cells (data not shown). In those portions of the dendritic arbor that stratify in the dendritic arbor's ultimate layer of the IPL, PSD95-GFP puncta were numerous (Figure 2 C-E). (The absence of puncta in the primary dendrites *en passage* also serves as evidence against the possibility of some sort of non-specific precipitation or aggregation of PSD95-GFP. For some other proteins, non-specific aggregation of proteins does occur, but it typically creates the opposite distribution, being greatest those dendrites that lie closest to the site of protein synthesis in the soma — data not shown.)

PSD95-GFP puncta were found in close apposition to known synaptic structures on both the presynaptic and the postsynaptic sides. Ganglion cells receive most of their excitatory input from bipolar cells, which are distinguished by the presence of synaptic ribbons. We counterstained transfected retinas with antibodies against the synaptic ribbon components Kif3a (kinesin II, Muresan et al., 1999) or RIBEYE (CtBP2, Schmitz et al., 2000). Almost all PSD95-GFP puncta were in close apposition to synaptic ribbons (Figure 3 A). These puncta represent zones where excitatory input occurs, but do not necessarily represent single excitatory synapses. There are many instances in which the PSD95-GFP punctum is associated with only a single presynaptic ribbon (arrows in Figure 3 A). But there is a conspicuous minority of cases where the PSD95-GFP punctum is clearly associated with two or more ribbons (arrowheads in Figure 3 A). In Figure 3 A, two long dendrites of the same cell are shown. Of the 34 PSD95-GFP puncta shown in the figure, 21 appear to represent individual synapses. In 12 cases the PSD95-GFP punctum, usually one of the larger ones, is associated with two or more ribbons. Only one punctum did not appear associated with any ribbon at all. Nearby pairs ("doublets") of ribbon synapses upon ganglion cells have been observed by electron microscopy (Famiglietti, 2005). The postsynaptic densities thus represent synaptic recipient zones rather than identifying individual synapses.

We evaluated the co-localization of PSD95-GFP with Kif3a labeling on a DS-cell quantitatively by averaging the pixel intensities in the PSD95-GFP (green) and the Kif3a (magenta) channel in 21×21 pixel squares surrounding the centroid of each PSD95-GFP punctum. The resulting plots quantify the tendency of a Kif3A punctum to occur near a PSD95-GFP punctum (Li et al., 2002). There was a strong tendency to co-occurrence of the two markers; it disappeared when, as a control, one of the two channels was rotated by 90 deg (Figure 3 E-F). Thus, there is a clear association of synaptic ribbons with PSD95-GFP puncta.

AMPA receptors underlie much of the synaptic transmission from bipolar cells to ganglion cells (Lukasiewicz et al., 1997), and almost all ganglion cells express GluR2 or GluR3 or both, though not necessarily on all of their synapses. Most ganglion cells express other AMPA receptor subtypes as well (Jeong et al., 2006; Jakobs et al., 2007). As shown in Figure 3 B and G, many, but not all, of the PSD95-GFP puncta on this cell (an ON-OFF DS cell) are co-localized with GluR2/3 immunoreactivity. It is also obvious from Figure 3 that labeled dendrites and synaptic structures are not distributed evenly but run in fascicles around the unlabeled profiles of Mueller cells (arrows in Figure 3 G). This presents a potential problem for our analysis, since structures that are localized in the same fascicle might falsely be found to be co-localized simply by virtue of their being necessarily close to each other. To test for this possibility, we performed double-labeling of PSD95-GFP expressing cells with GABAR-A, a receptor that should be expressed on most if not all ganglion cells, but is not expected to co-localize with PSD95. As shown in Figure 3 C and J, the cell's dendrites run in fascicles that are also brightly positive for GABAR-A. In the correlation plot (Figure 3 K) no peak is apparent, indicating the lack of correlation between these two markers. In summary, these experiments indicate that expression of PSD95-GFP — at least in the amount and for the times studied here — is a reliable way to identify the sites of excitatory synapses on retinal ganglion cells.

The functional diversity of ganglion cells is not accompanied by specialized local patterns of excitatory inputs

We collected confocal stacks in 0.4 μm steps of 56 ganglion cells gene gunned with PSD95-GFP. The image stacks were archived and inspected for suitability for digitization. Our criteria were (1) agreement on the cell type by three independent observers (two of the authors and one other experienced retinal anatomist) (2) minimal overlap of the dendritic arbor with that of other cells, (3) no signs of degeneration, and (4) Optimal conditions for imaging, i.e. very flat mounting and strong contrast. Out of the original sample, 25 cells met these criteria and 10 were digitized in the Neurolucida software package (Table 1). The major conclusions drawn from quantitative analysis could be verified visually by inspection of the larger series of cells. As a resource for future studies, we have made the image stacks of these 10 cells available at high resolution (see supplemental materials S1).

We chose for study a series of cell types (described in more detail under Methods) that span a wide range of physiological and structural properties. In brief, they are: The Local Edge Detector (LED), the smallest of all ganglion cells in the rabbit, which has highly non-linear response to spatial contrast; the G3 cell, a small bistratified neuron; the G5 cell, an OFF cell which has a distinctively flat arbor in layer 2 of the IPL and fires a transient burst of spikes at stimulus offset; the much studied ON — OFF directionally selective cell; the less numerous ON directionally selective cell; and the Brisk Transient cell, analogous in physiology to the Y cell of the cat, which is anatomically termed the alpha cell and is the largest ganglion cell in most retinas.

A striking feature of the distribution of excitatory synapses was how little it varied across the different types of cells; in pattern, in the regularity of their spacing, and even in absolute density (Table 1 and Figure 4). These cells span the entire range of receptive field sizes in the rabbit and include cells with relatively simple receptive field characteristics and cells whose responses to light include complex non-linearities. Nonetheless, the density of excitatory inputs varied by less than a factor of two, from 0.15 puncta per linear μm of dendrite to 0.28 puncta / μm. This was the case despite dramatic differences in the cells' physiology, an order of magnitude range of total dendritic length, and widely differing patterns of dendritic branching (Figure 4 and 5).

Likewise, the spatial distribution of synapses was similar across cells. As noted above, synapses avoided the dendrites that traversed the levels of the inner plexiform layer, linking arbors of bistratified cells or the soma and a monostratified arbor. Otherwise, there was little difference between the pattern of excitatory input to lower order dendritic segments and higher (Figure 5). The few cell types that have been reconstructed by electron microscopy (in cat and monkey) showed the same absence of pattern of excitatory inputs (Sterling, 1983;McGuire et al., 1986;Cohen and Sterling, 1991;Jacoby et al., 1996;Calkins et al., 1998;Jacoby et al., 2000). Across the whole sample of reconstructed cells the total density of PSD95-GFP puncta was 0.19 ± 0.04 puncta/linear μm, a narrow range for cells of such diverse size and physiology (Table 1). The variations in the mean value did not correlate with any evident characteristic of the cells, such as size or complexity of the cell type's physiological responses; nor did it vary for different spatial locations within the dendritic arbors.

The spatial densities of cone bipolar outputs vary little across the inner plexiform layer

One of our major findings is that the dendritic arbors of different types of retinal ganglion cells receive synapses at a similar linear density, independent of the size or physiological type of the ganglion cell. Because retinal ganglion cells of different types arborize at differing depths of the inner plexiform layer, the finding offers a test of the veracity of PSD95-GFP as a marker of the sites of excitatory input. Most, if not all, excitatory inputs to retinal ganglion cells are accompanied on the presynaptic side by a synaptic ribbon, the characteristic specialization of synapses formed by retinal bipolar cell axons. Thus, if the postsynaptic density of inputs to retinal ganglion cells varied little among cell types that arborize at different levels of the inner plexiform layer, then the density of ribbon synapses at those same levels of the inner plexiform layer should also vary little.

If each layer of the IPL were occupied exclusively by the dendrites of a single ganglion cell type, then the spatial densities of PSD95 puncta and synaptic ribbons should match. We therefore measured the density of synaptic ribbons, indicated by immunostaining for RIBEYE, at a series of depths of the IPL (Figure 6). For layers 1-4 of the IPL the density of synaptic ribbons ranged only from 15.98×10^4 / mm^2 to 20.07×10^4 /mm^2. (Layer five is dominated by axon terminals of the rod bipolar cells, which make few if any synapses upon retinal ganglion cells, so the ribbon density in this layer is less informative for our analysis.) Although a one-for-one matching of presynaptic and postsynaptic elements is not yet possible for individual cell types, the finding again suggests a relative uniformity of the excitatory inputs.

Distribution of PSD95 sites within the receptive field

The measurements described above were of the linear distribution of input sites along the dendrites. We also analyzed their overall distribution in two dimensional space, relative only to the cell's soma. The method of measurement is summarized in Figure 7. For all but one of the cell types studied, there was a distinctive peak in the density of inputs at distances slightly removed from the cell soma. This is similar to the familiar Gaussian shaped receptive field center that has been described for retinal ganglion cells, with the exception that we observe a dip in the center of the distribution (Figure 7). The dip is caused by the paucity of inputs to the most proximal dendrites (Figures 2 and 4).

We also computed simply the total density of PSD95 sites as a function of the area of the dendritic field. We found a strong inverse relationship (Figure 8); such that the receptive fields of small cells receive far denser excitatory inputs than large ones. This relationship held for all of the cell types studied. It also held for two cells that belonged to the same functional type (ON-OFF directionally selective cells) but had different dendritic field size

by virtue of their location at different retinal eccentricity. This suggests that the relationship depends on arbor size *per se*, rather than ganglion cell type.

Discussion

These studies rely upon transfection of the cell with a plasmid coding for a PSD95 — GFP fusion protein as a way to identify the ganglion cell's synaptic input zones. There is much published precedent for use of labeled PSD95 in this way (Arnold and Clapham, 1999; Marrs et al., 2001; Ebihara et al., 2003), including recent studies in the retina by Morgan et al., (2008), who verified the conclusion electrophysiologically. Our evidence is that synaptic function, as judged by neuronal structure and responses to light, was normal in these intact retinas. While we have observed cases where overexpression of some other proteins results in an inappropriate synthesis or targeting of those proteins, we have four reasons to believe that this did not happen for PSD95-GFP: (1) The localization of PSD95-GFP was stable over time and was highly reproducible from experiment to experiment. (2) Although the PSD95-GFP was localized throughout most of the dendritic arbors, it was not present indiscriminately: The proximal dendrites, which cross the inner plexiform layer to reach their final stratification, contained few PSD95-GFP puncta. (3) In those cases where the results could be directly compared with electron microscopic localization (Famiglietti, 2005), the patterns of synapses observed was consistent with that seen by expression of PSD95-GFP. (4) PSD95-GFP puncta were co localized with other markers of excitatory synapses: Kif 3a and RIBEYE as markers of ribbon synapses on the presynaptic side; and GluR2/3 on the postsynaptic side.

Profiles of receptive field sensitivity and the distribution of excitatory inputs

When we analyzed the distribution of input sites across the two dimensional area surveyed by the dendritic field, two generalizations emerged. The first was that, for all but one (particularly asymmetric) arbor, the maximal density of PSD95 sites occurred in a ring shaped area surrounding the cell soma. Since the density of PSD95 sites on the dendrites varies little throughout the dendritic arbor, this areal distribution reflects different spatial densities of the dendrites at different distances. In other words, the dendritic arbor is not perfectly space-filling: there is a region near the soma where the density of dendrites is especially high. The coverage of the retina by bipolar cells is essentially uniform (every known bipolar cell type has a coverage factor near unity (see (MacNeil et al., 2004) and references therein), so that the sensitivity profile of the bipolar cell output to the ganglion cells is essentially flat -- there are no major irregularities in the bipolar cell mosaic. Thus, the ultimate sensitivity of the ganglion cell should be determined by the number of bipolar inputs upon that cell's dendritic arbor and the physiological sensitivity of the cell should peak where that number is highest. In fact, modeling of the inputs from bipolar cells to alpha ganglion cells in the cat predicted the known Gaussian-like falloff of sensitivity, but the simulation showed a notch near the region of the soma (Freed et al., 1992). In the rabbit, receptive fields of individual ganglion cells have been directly mapped at very high resolution: the depression of sensitivity over the cell soma, predicted here by the absence of PSD95 sites on the most proximal dendrites, was in fact observed for many of the cells (see Figures 1,3,4,5,7, and 8 of Brown and Masland, 2000). It is interesting that this match occurred without any particular weighting of the strengths of the input, supporting the earlier prediction (Freed et al., 1992) that the ganglion cells are electrotonically compact, and suggesting that the strengths of the synapses at each PSD95 site are more or less equivalent.

Small cells receive more excitation per unit area of their receptive fields

We uncovered a strong ($r = -0.89$) inverse relationship between the area enclosed by a ganglion cell's dendritic field and the density of synapses per unit area: small cells receive

denser synaptic inputs than large ones (Figure 8). This relationship is not determined primarily by cell type. Although different cell types do have different sizes for any given retinal eccentricity, our sample also includes two examples of the ON-OFF direction selective cell, one from the central retina and one from the peripheral. Even though their areas differ by ~ 300%, both have the overall density of PSD95 sites predicted by the general relationship. Nor is the relationship a matter of how thickly stratified the cell type is, as both the LED and the brisk transient cell are highly stratified. This is a counterintuitive finding, because individual synapses upon small cells should, if anything, be more powerful biophysically in depolarizing the soma than synapses on large ones.

The structural basis of this relationship is, as for the sensitivity profile, that small cells have more dendrite per unit retinal area than large ones. An interpretation of its functional significance is as follows. If the ganglion cells are electrotonically compact, as discussed above, and if all of their excitatory inputs are roughly equal in effectiveness, then the total excitatory drive available to move the membrane potential toward the cell's threshold for action potentials depends simply upon the total number of synapses that each cell receives. Yet, some cells survey large regions of the world and others small regions. If the cells received the same areal density of synaptic inputs, the problem is that the small cells would receive far less total excitatory drive than the large ones, since the areas of the receptive fields can vary by more than an order of magnitude. In the absence of other compensations, then, the small ganglion cells would be far less sensitive to stimulation of the retina with light than the large ones. This tendency will be counteracted by increased spatial density of inputs to small cells. In other words, the differential density of excitatory inputs will tend to normalize the responses of small cells and large ones -- to bring the the response of a small cell and a large cell into the same dynamic range. Otherwise, a stimulus that entirely covers both receptive fields would drive the large cell far more strongly than that same stimulus drives the small cell. Many other kinds of compensation can of course be imagined and our interpretation is likely to be a simplification. If nothing else, though, the present results point out the existence of the problem.

Comparison with other species: the synaptic distributions of mammalian ganglion cells follow a single generic plan

The ganglion cells of the rabbit have been studied in detail electrophysiologically and for many the response properties have been unambiguously linked to defined morphological types (Levick, 1967; Caldwell and Daw, 1978; Amthor et al., 1989a; Amthor et al., 1989b; Rockhill et al., 2002; Roska et al., 2006). They range from the large and straightforward brisk transient cell to the tiny but physiologically complex local edge detector. And yet, we find a similar pattern of excitatory input to all cell types. The two small cell types that have been reconstructed by serial section electron microscopy (in cat and monkey) showed the same absence of pattern of excitatory inputs. Surprisingly, given their difference in size, this extends even to the absolute density of excitatory input zones, which ranged over less than a factor of two for our whole sample of cell types.

A study similar to the present one in scope and goals has recently been reported in the guinea pig (Xu et al., 2008). Our fundamental findings in the rabbit are in agreement: all types of retinal ganglion cell show a uniform distribution of excitatory inputs (these were measured by Xu et al. by staining synaptic ribbons and associating them computationally with the dendrites of injected cells.) They report a "dome shaped" distribution of synaptic inputs across the dendritic field, where we see a drop in synaptic density near the center of the receptive field. However, this is clearly due to smoothing of their data across the region of the soma and proximal dendrites (see their figure 4). A uniform distribution of excitatory synaptic inputs around the dendritic arbor has also been reported for midget, parasol, and "garland" cells of the macaque monkey (Cohen and Sterling, 1991; Jacoby et al., 1996;

Calkins et al., 1998; Calkins and Sterling, 2007); for midget, parasol, melanopsin-expressing and blue-On cells of the marmoset monkey (Ghosh and Grünert, 1999; Jusuf et al., 2007; Eriköz et al., 2008) ; and for alpha and beta cells of the cat retina (McGuire et al., 1986; Freed and Sterling, 1988). Inhibitory synapses appear to follow the same rules, though the conclusion is at present limited by the lack of a cytochemical marker that would reveal all of the types of inhibitory synapse. (Calkins et al., 1998; Grünert and Ghosh, 1999; Jeon et al., 2002; Lin et al., 2002). Where they can be compared, results from light and electron microscopy agree. The pattern described here and in these previous papers — from different laboratories and using different methodologies -- seems to represent the unambiguous description of a generic mammalian plan for distributing synaptic inputs to retinal ganglion cells.

It is ironic that influential early speculations about dendritic computation (Torre and Poggio, 1978; Koch et al., 1983; Koch et al., 1987) focused on the dendritic trees of retinal ganglion cells, which now seem fairly simple, at least in their pattern of inputs. In this regard, retinal ganglion cells appear different from many other projection neurons, in which different regions of the dendritic arbor receive different densities and types of excitatory and inhibitory synaptic input, and where the types of interactions once postulated for retinal ganglion cells are easily demonstrated. This is not to say that dendritic computations do not occur in retinal ganglion cells -- only that they are not based upon the spatial arrangement of inputs. An unequivocal example of dendritic specialization is variation in the expression of ion channels (O'Brien et al., 2002; Oesch et al., 2005). O'Brien and colleagues carefully correlated the morphological types of cat ganglion cells with the array of ionic conductances manifest in the cells. They found the conductances to represent biophysical signatures so distinctive that they uniquely characterize each cell type.

In summary, the generic retinal ganglion cell suggested by our results and others' is a compact neuron that does not achieve integrative function by the spatial patterning of excitation and inhibition within specialized regions of the dendritic arbor. Instead, its distinctive responses are created by combining excitatory and inhibitory inputs that have been pre processed by bipolar and amacrine cells. Those inputs, once collected, are shaped in distinctive ways by the cell-type-specific expression and spatial arrangement of ion channel proteins.

Resource sharing

Supplementary material 1 consists of an annotated set of 10 image stacks showing individual retinal ganglion cells expressing PSD95 — GFP. The cells were imaged at high resolution in z steps of 0.4 μm. Where possible, the cells are identified by functional type.

Acknowledgments

We thank Yixin Ben for gene gunning and retina incubation, Rebecca Rockhill for creating digital representations of the confocal image stacks, and Bingxing Huo for help with the preparation of figures. RHM is a Senior Investigator of Research to Prevent Blindness. Supported by NIH grant R01-EY017169.

This work has been supported by a NIH grant (R01-EY017169).

References

Amthor FR, Oyster CW, Takahashi ES. Morphology of on-off direction-selective ganglion cells in the rabbit retina. Brain Res. 1984; 298:187–190. [PubMed: 6722555]

Amthor FR, Takahashi ES, Oyster CW. Morphologies of rabbit retinal ganglion cells with complex receptive fields. J Comp Neurol. 1989a; 280:97–121. [PubMed: 2918098]

Amthor FR, Takahashi ES, Oyster CW. Morphologies of rabbit retinal ganglion cells with concentric receptive fields. J Comp Neurol. 1989b; 280:72–96. [PubMed: 2918097]

Arnold DB, Clapham DE. Molecular determinants for subcellular localization of PSD-95 with an interacting K+ channel. Neuron. 1999; 23:149–157. [PubMed: 10402201]

Barlow H, Levick W. The mechanism of directionally selective units in rabbit's retina. J Physiol. 1965; 178:477–504. [PubMed: 5827909]

Brown SP, Masland RH. Receptive field microstructure and dendritic geometry of retinal ganglion cells. Neuron. 2000; 27:371–383. [PubMed: 10985356]

Caldwell JH, Daw NW. New properties of rabbit retinal ganglion cells. J Physiol. 1978; 276:257–276. [PubMed: 650447]

Calkins DJ, Sterling P. Absence of spectrally specific lateral inputs to midget ganglion cells in the primate retina. Nature. 1996; 381:613–615. [PubMed: 8637598]

Calkins DJ, Sterling P. Microcircuitry for two types of achromatic ganglion cell in primate fovea. J Neurosci. 2007; 27:2646–2653. [PubMed: 17344402]

Calkins DJ, Tsukamoto Y, Sterling P. Microcircuitry and mosaic of a blue-yellow ganglion cell in the primate retina. J Neurosci. 1998; 18:3373–3385. [PubMed: 9547245]

Cleland BG, Levick WR. Brisk and sluggish concentrically organized ganglion cells in the cat's retina. J Physiol. 1974; 240:421–456. [PubMed: 4421622]

Cohen E, Sterling P. Microcircuitry related to the receptive field center of the on-beta ganglion cell. J Neurophysiol. 1991; 65:352–359. [PubMed: 2016645]

Dacey DM. Morphology of a small-field bistratified ganglion cell type in the macaque and human retina. Vis Neurosci. 1993; 10:1081–1098. [PubMed: 8257665]

Dacheux RF, Chimento MF, Amthor FR. Synaptic input to the on-off directionally selective ganglion cell in the rabbit retina. J Comp Neurol. 2003; 456:267–278. [PubMed: 12528191]

Ebihara T, Kawabata I, Usui S, Sobue K, Okabe S. Synchronized formation and remodeling of postsynaptic densities: long-term visualization of hippocampal neurons expressing postsynaptic density proteins tagged with green fluorescent protein. J Neurosci. 2003; 23:2170–2181. [PubMed: 12657676]

Eriköz B, Jusuf PR, Percival KA, Grünert U. Distribution of bipolar input to midget and parasol ganglion cells in marmoset retina. Vis Neurosci. 2008; 25:67–76. [PubMed: 18282311]

Famiglietti EV. Synaptic organization of complex ganglion cells in rabbit retina: type and arrangement of inputs to directionally selective and local-edge-detector cells. J Comp Neurol. 2005; 484:357–391. [PubMed: 15770656]

Freed MA, Smith RG, Sterling P. Computational model of the on-alpha ganglion cell receptive field based on bipolar cell circuitry. Proc Natl Acad Sci USA. 1992; 89:236–240. [PubMed: 1309606]

Freed MA, Sterling P. The ON-alpha ganglion cell of the cat retina and its presynaptic cell types. J Neurosci. 1988; 8:2303–2320. [PubMed: 3249227]

Fried SI, Münch TA, Werblin FS. Mechanisms and circuitry underlying directional selectivity in the retina. Nature. 2002; 420:411–414. [PubMed: 12459782]

García-López P, García-Marín V, Freire M. Three-dimensional reconstruction and quantitative study of a pyramidal cell of a Cajal histological preparation. J Neurosci. 2006; 26:11249–11252. [PubMed: 17079652]

Ghosh KK, Grünert U. Synaptic input to small bistratified (blue-ON) ganglion cells in the retina of a new world monkey, the marmoset Callithrix jacchus. J Comp Neurol. 1999; 413:417–428. [PubMed: 10502249]

Grünert U, Ghosh KK. Midget and parasol ganglion cells of the primate retina express the alpha1 subunit of the glycine receptor. Vis Neurosci. 1999; 16:957–966. [PubMed: 10580731]

Gulyas AI, Megias M, Emri Z, Freund TF. Total number and ratio of excitatory and inhibitory synapses converging onto single interneurons of different types in the CA1 area of the rat hippocampus. J Neurosci. 1999; 19:10082–10097. [PubMed: 10559416]

He S, Masland RH. ON direction-selective ganglion cells in the rabbit retina: dendritic morphology and pattern of fasciculation. Vis Neurosci. 1998; 15:369–375. [PubMed: 9605536]

Hildebrand JD, Soriano P. Overlapping and unique roles for C-terminal binding protein 1 (CtBP1) and CtBP2 during mouse development. Mol Cell Biol. 2002; 22:5296–5307. [PubMed: 12101226]

Hirano AA, Brandstätter JH, Vila A, Brecha NC. Robust syntaxin-4 immunoreactivity in mammalian horizontal cell processes. Vis Neurosci. 2007; 24:489–502. [PubMed: 17640443]

Jacoby R, Stafford D, Kouyama N, Marshak D. Synaptic inputs to ON parasol ganglion cells in the primate retina. J Neurosci. 1996; 16:8041–8056. [PubMed: 8987830]

Jacoby RA, Wiechmann AF, Amara SG, Leighton BH, Marshak DW. Diffuse bipolar cells provide input to OFF parasol ganglion cells in the macaque retina. J Comp Neurol. 2000; 416:6–18. [PubMed: 10578099]

Jakobs TC, Ben Y, Masland RH. Expression of mRNA for glutamate receptor subunits distinguishes the major classes of retinal neurons, but is less specific for individual cell types. Mol Vis. 2007; 13:933–948. [PubMed: 17653033]

Jeon CJ, Kong JH, Strettoi E, Rockhill R, Stasheff SF, Masland RH. Pattern of synaptic excitation and inhibition upon direction-selective retinal ganglion cells. J Comp Neurol. 2002; 449:195–205. [PubMed: 12115689]

Jeong SA, Kwon OJ, Lee JY, Kim TJ, Jeon CJ. Synaptic pattern of AMPA receptor subtypes upon direction-selective retinal ganglion cells. Neurosci Res. 2006; 56:427–434. [PubMed: 17007948]

Jusuf PR, Lee SC, Hannibal J, Grünert U. Characterization and synaptic connectivity of melanopsin-containing ganglion cells in the primate retina. Eur J Neurosci. 2007; 26:2906–2921. [PubMed: 18001286]

Jusuf PR, Martin PR, Grünert U. Synaptic connectivity in the midget-parvocellular pathway of primate central retina. J Comp Neurol. 2006; 494:260–274. [PubMed: 16320234]

Klug K, Herr S, Ngo IT, Sterling P, Schein S. Macaque retina contains an S-cone OFF midget pathway. J Neurosci. 2003; 23:9881–9887. [PubMed: 14586017]

Koch, C.; Poggio, T.; Edelman, GM.; Gall, WE.; Cowan, WM. Synaptic Function. Wiley-Interscience; New York, N.Y.: 1987. Biophysics of computation: neurons, synapses, and membranes; p. 637-697.

Koch C, Poggio T, Torre V. Nonlinear interactions in a dendritic tree: Localizaion, timing, and role in information processing. Proc Natl Acad Sci USA. 1983; 80:2799–2802. [PubMed: 6573680]

Koizumi A, Jakobs TC, Masland RH. Inward rectifying currents stabilize the membrane potential in dendrites of mouse amacrine cells: patch-clamp recordings and single-cell RTPCR. Mol Vis. 2004; 10:328–340. [PubMed: 15152185]

Koizumi A, Zeck G, Ben Y, Masland RH, Jakobs TC. Organotypic culture of physiologically functional adult Mammalian retinas. PLoS ONE. 2007; 2:e221. [PubMed: 17311097]

Koulen P, Sassoè-Pognetto M, Grünert U, Wässle H. Selective clustering of GABA(A) and glycine receptors in the mammalian retina. J Neurosci. 1996; 16:2127–2140. [PubMed: 8604056]

Levick WR. Receptive fields and trigger features of ganglion cells in the visual streak of the rabbit's retina. J Physiol. 1967; 188:285–307. [PubMed: 6032202]

Li W, Trexler EB, Massey SC. Glutamate receptors at rod bipolar ribbon synapses in the rabbit retina. J Comp Neurol. 2002; 448:230–248. [PubMed: 12115706]

Lin B, Martin PR, Grünert U. Expression and distribution of ionotropic glutamate receptor subunits on parasol ganglion cells in the primate retina. Vis Neurosci. 2002; 19:453–465. [PubMed: 12511078]

Lin B, Martin PR, Solomon SG, Grünert U. Distribution of glycine receptor subunits on primate retinal ganglion cells: a quantitative analysis. Eur J Neurosci. 2000; 12:4155–4170. [PubMed: 11122328]

Lo DC, McAllister AK, Katz LC. Neuronal transfection in brain slices using particle-mediated gene transfer. Neuron. 1994; 13:1263–1268. [PubMed: 7993619]

Lukasiewicz PD, Wilson JA, Lawrence JE. AMPA-preferring receptors mediate excitatory synaptic inputs to retinal ganglion cells. J Neurophysiol. 1997; 77:57–64. [PubMed: 9120596]

MacNeil MA, Heussy JK, Dacheux RF, Raviola E, Masland RH. The population of bipolar cells in the rabbit retina. J Comp Neurol. 2004; 472:73–86. [PubMed: 15024753]

Macri J, Martin PR, Grünert U. Distribution of the alpha1 subunit of the GABA(A) receptor on midget and parasol ganglion cells in the retina of the common marmoset Callithrix jacchus. Vis Neurosci. 2000; 17:437–448. [PubMed: 10910110]

Marrs GS, Green SH, Dailey ME. Rapid formation and remodeling of postsynaptic densities in developing dendrites. Nature Neurosci. 2001; 4:1006–1013. [PubMed: 11574832]

Marshak DW, Yamada ES, Bordt AS, Perryman WC. Synaptic input to an ON parasol ganglion cell in the macaque retina: a serial section analysis. Vis Neurosci. 2002; 19:299–305. [PubMed: 12392179]

Masland RH. The fundamental plan of the retina. Nature Neurosci. 2001; 4:877–886. [PubMed: 11528418]

McGuire BA, Stevens JK, Sterling P. Microcircuitry of beta ganglion cells in cat retina. J Neurosci. 1986; 6:907–918. [PubMed: 3701415]

Megias M, Emri Z, Freund TF, Gulyas AI. Total number and distribution of inhibitory and excitatory synapses on hippocampal CA1 pyramidal cells. Neuroscience. 2001; 102:527–540. [PubMed: 11226691]

Morgan JL, Schubert T, Wong ROL. Developmental patterning of glutamatergic synapses onto retinal ganglion cells. Neural Develop. 2008; 3:8. [PubMed: 18366789]

Muresan V, Lyass A, Schnapp BJ. The kinesin motor KIF3A is a component of the presynaptic ribbon in vertebrate photoreceptors. J Neurosci. 1999; 19:1027–1037. [PubMed: 9920666]

O'Brien BJ, Isayama T, Richardson R, Berson DM. Intrinsic physiological properties of cat retinal ganglion cells. J Physiol. 2002; 538(Pt 3):787–802. [PubMed: 11826165]

Oesch N, Euler T, Taylor WR. Direction-selective dendritic action potentials in rabbit retina. Neuron. 2005; 47:739–750. [PubMed: 16129402]

Owczarzak MT, Pourcho RG. Transmitter-specific input to OFF-alpha ganglion cells in the cat retina. Anat Rec. 1999; 255:363–373. [PubMed: 10409808]

Oyster CW, Simpson JI, Takahashi ES, Soodak RE. Retinal ganglion cells projecting to the rabbit accessory optic system. J Comp Neurol. 1980; 190:49–61. [PubMed: 7381054]

Peichl L, Buhl EH, Boycott BB. Alpha ganglion cells in the rabbit retina. J Comp Neurol. 1987; 263:25–41. [PubMed: 2444630]

Rissman RA, Mishizen-Eberz AJ, Carter TL, Wolfe BB, De Blas AL, Miralles CP, Ikonomovic MD, Armstrong DM. Biochemical analysis of GABA(A) receptor subunits alpha 1, alpha 5, beta 1, beta 2 in the hippocampus of patients with Alzheimer's disease neuropathology. Neuroscience. 2003; 120:695–704. [PubMed: 12895510]

Rockhill RL, Daly FJ, MacNeil MA, Brown SP, Masland RH. The diversity of ganglion cells in a mammalian retina. J Neurosci. 2002; 22:3831–3843. [PubMed: 11978858]

Roska B, Molnar A, Werblin FS. Parallel processing in retinal ganglion cells: how integration of space-time patterns of excitation and inhibition form the spiking output. J Neurophysiol. 2006; 95:3810–3822. [PubMed: 16510780]

Roska B, Werblin F. Vertical interactions across ten parallel, stacked representations in the mammalian retina. Nature. 2001; 410:583–587. [PubMed: 11279496]

Sanchez AL, Matthews BJ, Meynard MM, Hu B, Javed S, Cory S Cohen. BDNF increases synapse density in dendrites of developing tectal neurons in vivo. Development. 2006; 133:2477–2486. [PubMed: 16728478]

Sassoè-Pognetto M, Kirsch J, Grünert U, Greferath U, Fritschy JM, Möhler H, Betz H, Wässle H. Colocalization of gephyrin and GABAA-receptor subunits in the rat retina. J Comp Neurol. 1995; 357:1–14. [PubMed: 7673460]

Schmitz F, Königstorfer A, Südhof TC. RIBEYE, a component of synaptic ribbons: a protein's journey through evolution provides insight into synaptic ribbon function. Neuron. 2000; 28:857–872. [PubMed: 11163272]

Sterling P. Microcircuitry of the cat retina. Ann Rev Neurosci. 1983; 6:149–185. [PubMed: 6838139]

tom Dieck S, Altrock WD, Kessels MM, Qualmann B, Regus H, Brauner D, Fejtova A, Bracko O, Gundelfinger ED, Brandstätter JH. Molecular dissection of the photoreceptor ribbon synapse: physical interaction of Bassoon and RIBEYE is essential for the assembly of the ribbon complex. J Cell Biol. 2005; 168:825–836. [PubMed: 15728193]

Torre V, Poggio T. A synaptic mechanism possibly underlying directional selectivity to motion. Proceedings of the Royal Society of LondonSeries B:Biological Science. 1978; 202:409–416.

van Wyk M, Taylor WR, Vaney DI. Local edge detectors: a substrate for fine spatial vision at low temporal frequencies in rabbit retina. J Neurosci. 2006; 26:13250–13263. [PubMed: 17182775]

Weber AJ, McCall MA, Stanford LR. Synaptic inputs to physiologically identified retinal X-cells in the cat. J Comp Neurol. 1991; 314:350–366. [PubMed: 1787179]

Weber AJ, Stanford LR. Synaptology of physiologically identified ganglion cells in the cat retina: a comparison of retinal X- and Y-cells. J Comp Neurol. 1994; 343:483–499. [PubMed: 8027453]

Wong RO, Herrmann K, Shatz CJ. Remodeling of retinal ganglion cell dendrites in the absence of action potential activity. J Neurobiol. 1991; 22:685–697. [PubMed: 1662709]

Xu Y, Vasudeva V, Vardi N, Sterling P, Freed MA. Different types of ganglion cell share a synaptic pattern. J Comp Neurol. 2008; 507:1871–1878. [PubMed: 18271025]

Yang G, Masland RH. Direct visualization of the dendritic and receptive fields of directionally selective retinal ganglion cells. Science. 1992; 258:1949–1952. [PubMed: 1470920]

Zeck GM, Xiao Q, Masland RH. The spatial filtering properties of local edge detectors and brisk-sustained retinal ganglion cells. Eur J Neurosci. 2005; 22:2016–2026. [PubMed: 16262640]

Zhang J, Diamond JS. Distinct perisynaptic and synaptic localization of NMDA and AMPA receptors on ganglion cells in rat retina. J Comp Neurol. 2006; 498:810–820. [PubMed: 16927255]

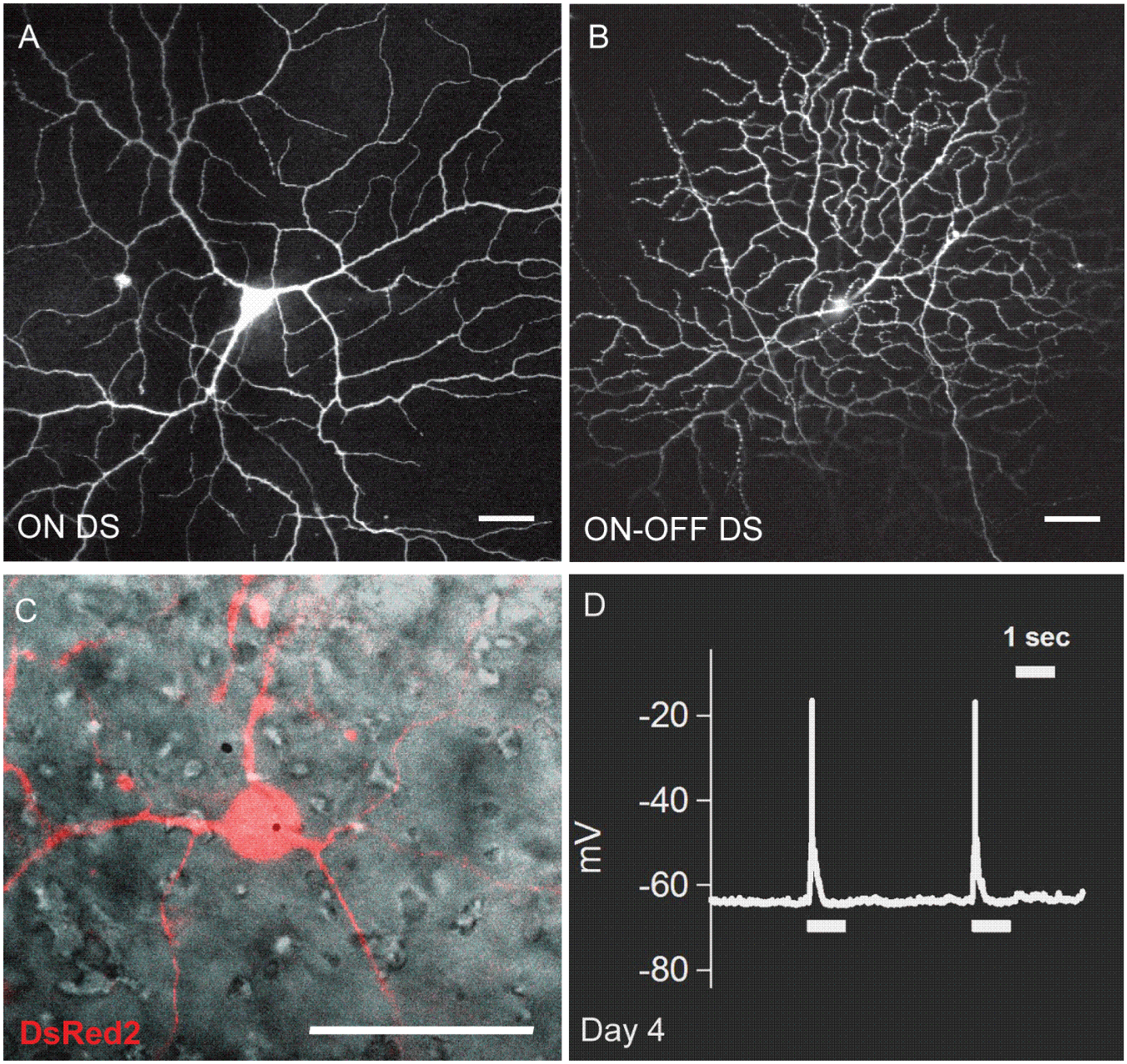

Figure 1. Retinal ganglion cells of retinas maintained in vitro for several days

(**A, B**) Normal morphology after 4 days. (**C, D**) responses to light after 4 days. (**C**) A cell expressing DsRed after gene gunning was targeted by fluorescence for recording. To avoid photodamage, the final electrode approach was guided by infra red DIC. This cell responded at the onset of illumination. Scale bar for panels A-C, 50 μm. (**D**). One second exposures to whole-field illumination at 1.6 cd/m^2.

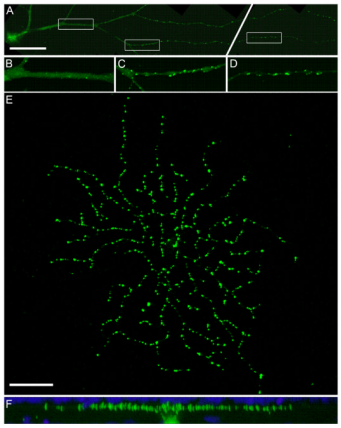

Figure 2. PSD95-GFP expression in retinal ganglion cells

(**A**) Main dendrite of a brisk-transient (alpha) ganglion cell expressing PSD95-GFP. The soma is visible on the left. A part of the dendrite has been cropped out (slanted bar) to allow simultaneous visualization of the proximal and distal parts. Scale bar, 50 μm. (**B-D**) Magnified view of the areas boxed in panel A. Synaptic zones labeled by PSD95-GFP appear as puncta of high pixel intensity. Note the almost complete absence of puncta on the proximal dendrite as compared to the medial (C) and distal (D) parts of the same dendrite. (**E**) The PSD95-GFP puncta of an G5 cell (OFF). Maximum intensity projection of 10 confocal image planes through the dendritic tree taken at 0.4 μm step size. For a view of the full image stack of this cell, see Suppl. Material S1 (cell 20041031-3). (**F**) Vertical projection of the same cell to show the depth of stratification. The inner nuclear layer (INL) and the ganglion cell layer (GCL) are visualized with the nuclear dye TOPRO (blue). Scale bar for E & F, 50 μm.

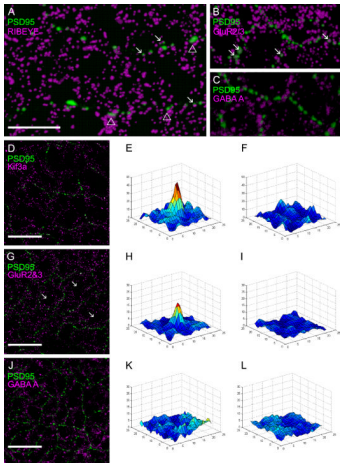

Figure 3. PSD95-GFP puncta are co-localized with pre- and postsynaptic markers

(**A**) Two dendrites of a ganglion cell are shown (labeled with PSD95-GFP, green), in tissue also immmunostained with an antibody against the synaptic ribbon component RIBEYE (magenta) showing the precise apposition of presynaptic (RIBEYE) and postsynaptic (PSD95-GFP) components. Arrows indicate PSD95-GFP labeled synaptic zones apposed to a single synaptic ribbon; arrowheads indicate broader synaptic zones contacting two or more ribbons. Volume reconstruction 20 image planes from a high-power image stack. Scale bar for panels A-C, 10 μm. (**B**) Volume reconstruction of the partial OFF-arbor of an ON/OFF DS cell labeled with PSD95-GFP (green) and anti-GluR2/3 (magenta). Due to the fact that both markers are post-synaptic, the signals overlap completely at some synaptic sites (arrows). Some PSD95 puncta are not colocalized with GluR2/3, suggesting that different receptor subunits are used at these sites. **(C)** Volume reconstruction of a partial OFF-arbor of an ON/OFF DS cell labeled with PSD95-GFP (green) and anti-GABAA receptor (magenta). **(D)** Single image plane of the dendritic arbor (partial) of a ganglion cell labeled with PSD95 (green) and Kif3a (magenta). Scale bar, 20 μm. (**E & F**) Correlation between PSD95-GFP in the green channel and Kif3a in the magenta (E), and between PSD95-GFP and Kif3a (F) with the magenta channel rotated by 90°, to identify the effect of random overlap (see methods). In these plots the central pixel represents the centroid of the PSD95-GFP puncta. The surrounding ones show the pixel intensity in the surrounding pixels in the magenta (Kif3a) channel (E), and the magenta channel rotated by 90° (F). Color code from dark blue (lowest intensity) to red (highest intensity). (**G**) Different ganglion cell, labeled with PSD95-GFP (green), and counterstained with an antibody against GluR2/3 (magenta). Scale bar, 20 μm. (**H & I**) Correlation between PSD95-GFP and GluR2/3 (F), and between PSD95-GFP and GluR2/3 with the magenta channel rotated by 90°. (**J**) different ganglion cell, labeled with PSD95-GFP and counterstained with anti-GABA-A receptor antibodies (magenta). Scale bar, 20 μm. (**K & L**) Spatial correlation of the two channels. Note the absence of a sharp correlation peak between PSD95-GFP and GABA-A.

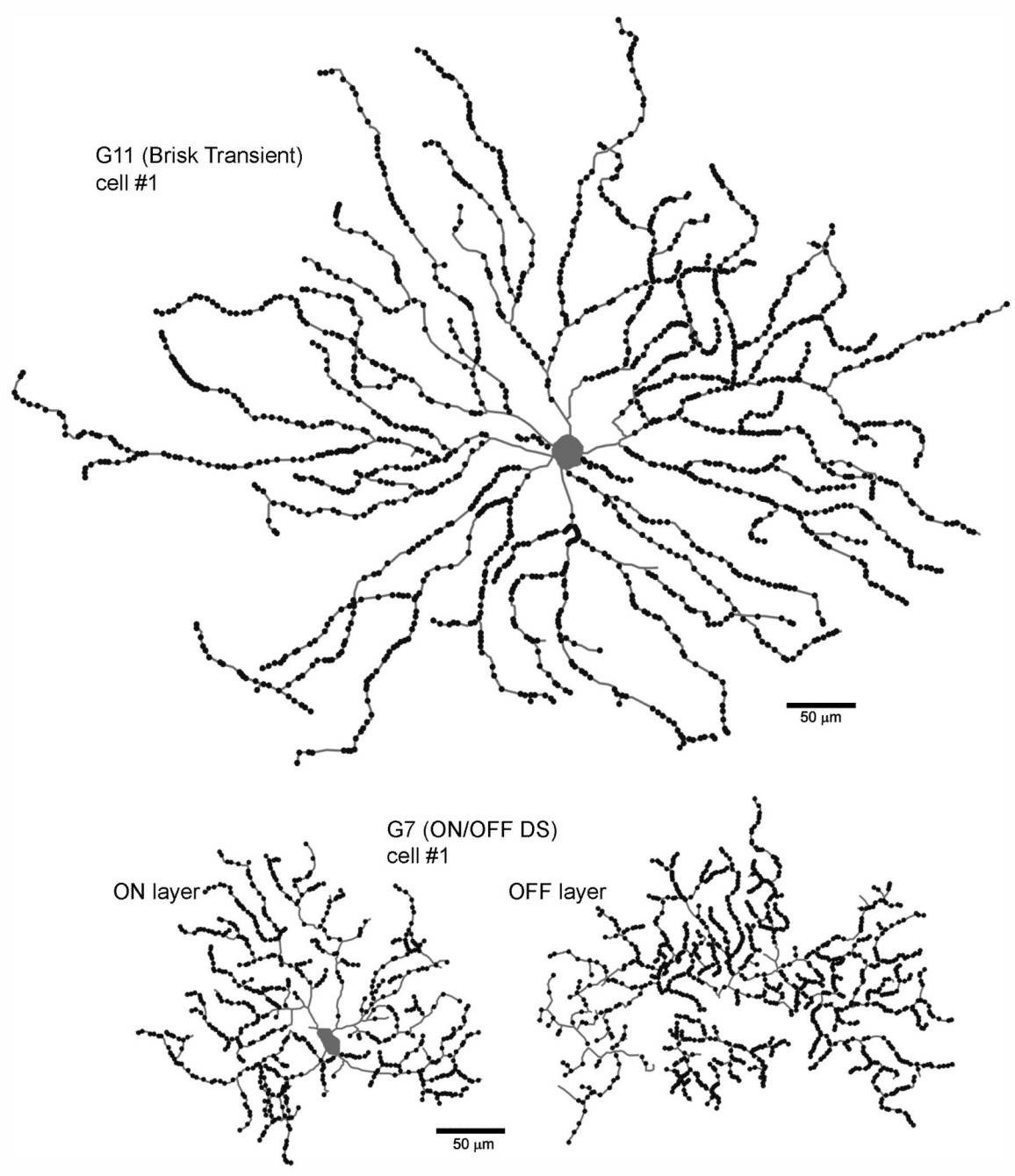

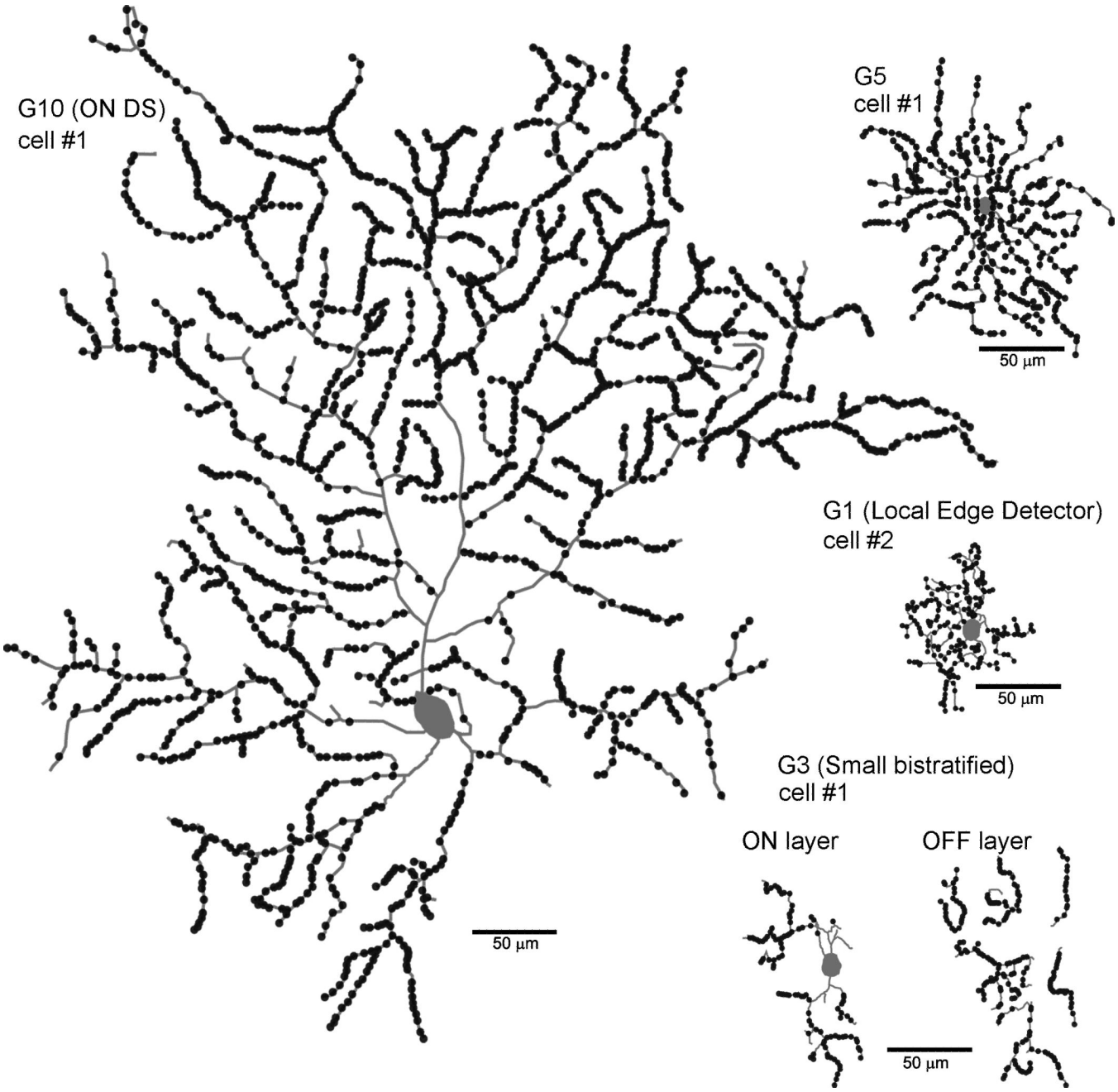

Figure 4. Synaptic input zones are uniformly distributed around the dendritic arbor of most types of ganglion cell

The sites of excitatory glutamatergic input (PSD95-GFP puncta) are indicated by dots. These are drawings from digital representations in Neurolucida software. Only one example for every cell type is shown. The cell ID numbers are the same as in table 1. The G5 cell #1 shown here was drawn from the raw data shown in Figure 2.

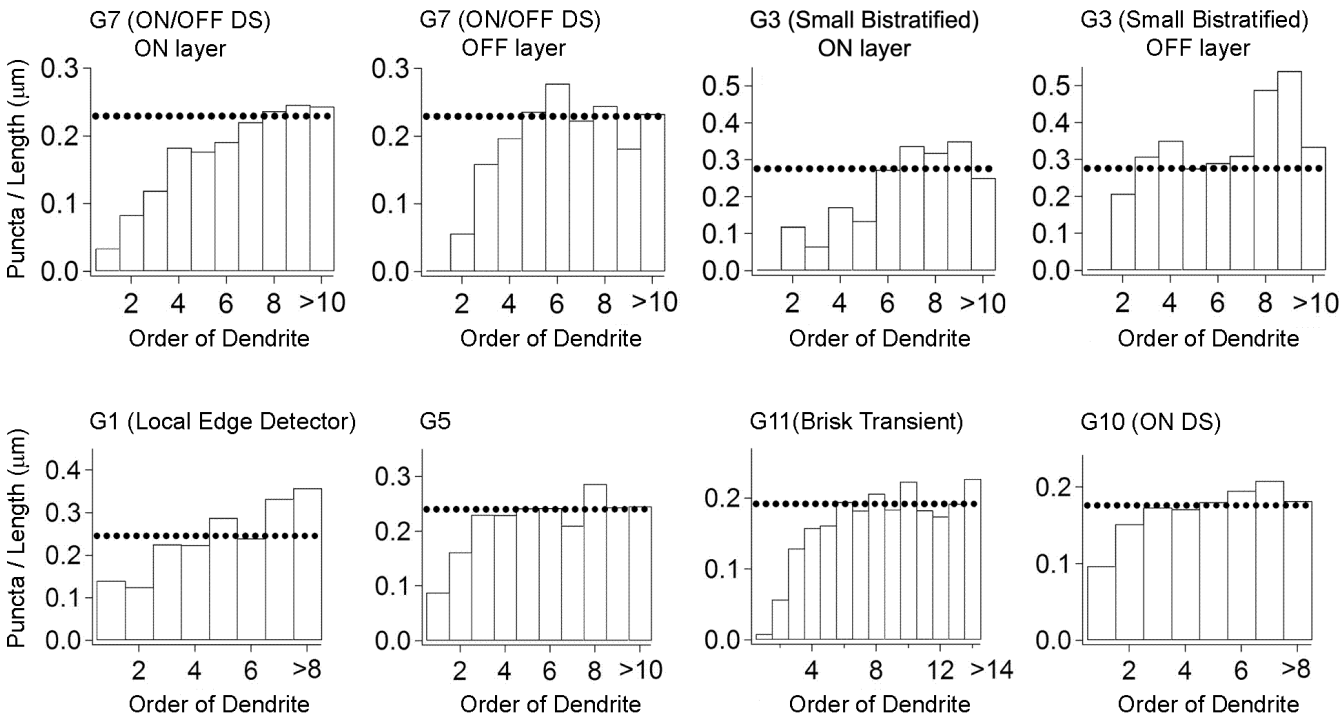

Figure 5. Density of excitatory synaptic inputs as a function of branch order

The first several orders — those connecting the soma with the eventual level of stratification -- have few inputs. Note that the final density of synaptic inputs, once outside the proximal zone, is similar for the different cell types, despite their widely differing sizes and physiologies.

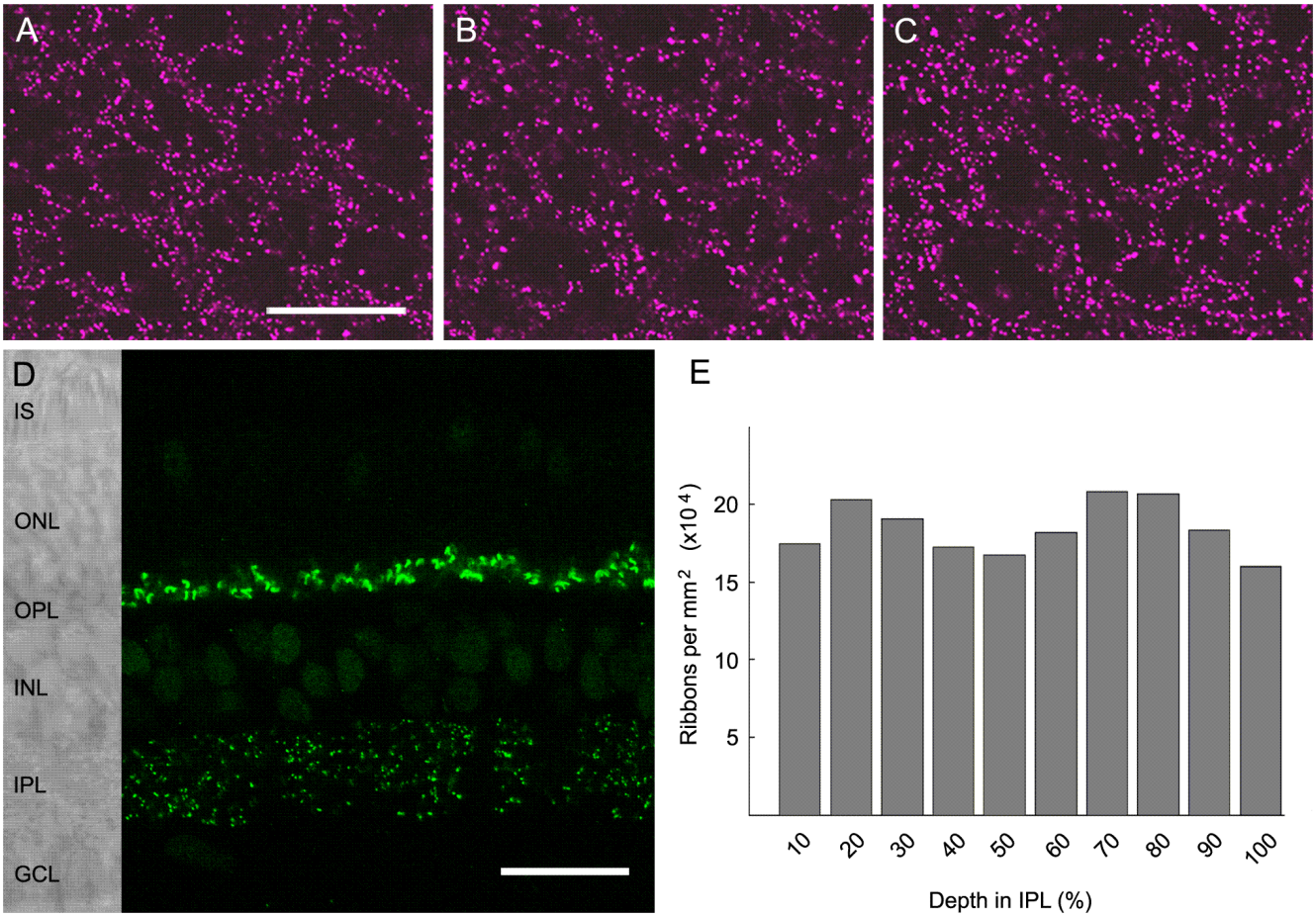

Figure 6. Distribution of synaptic ribbons in the inner plexiform layer

(A-C) Optical sections through the IPL at 20%, 50% and 80% depth. RIBEYE staining in magenta. Scale bar for all panels, 20 μm. **(D)** Vertical section through a rabbit retina stained for the synaptic ribbon marker RIBEYE (green). A DIC image is provided for orientation. The large structures in the OPL are ribbons associated with rod and cone terminals. The smaller punctate labeling in the IPL corresponds to the ribbons on bipolar axon terminals. Note that there is no obvious gradient of ribbon density in the IPL. Scale bar, 50 μm. **(E)** Number of synaptic ribbons per mm^2 as a function of IPL depth (0% is closest to the INL, 100% is closest to the GCL).

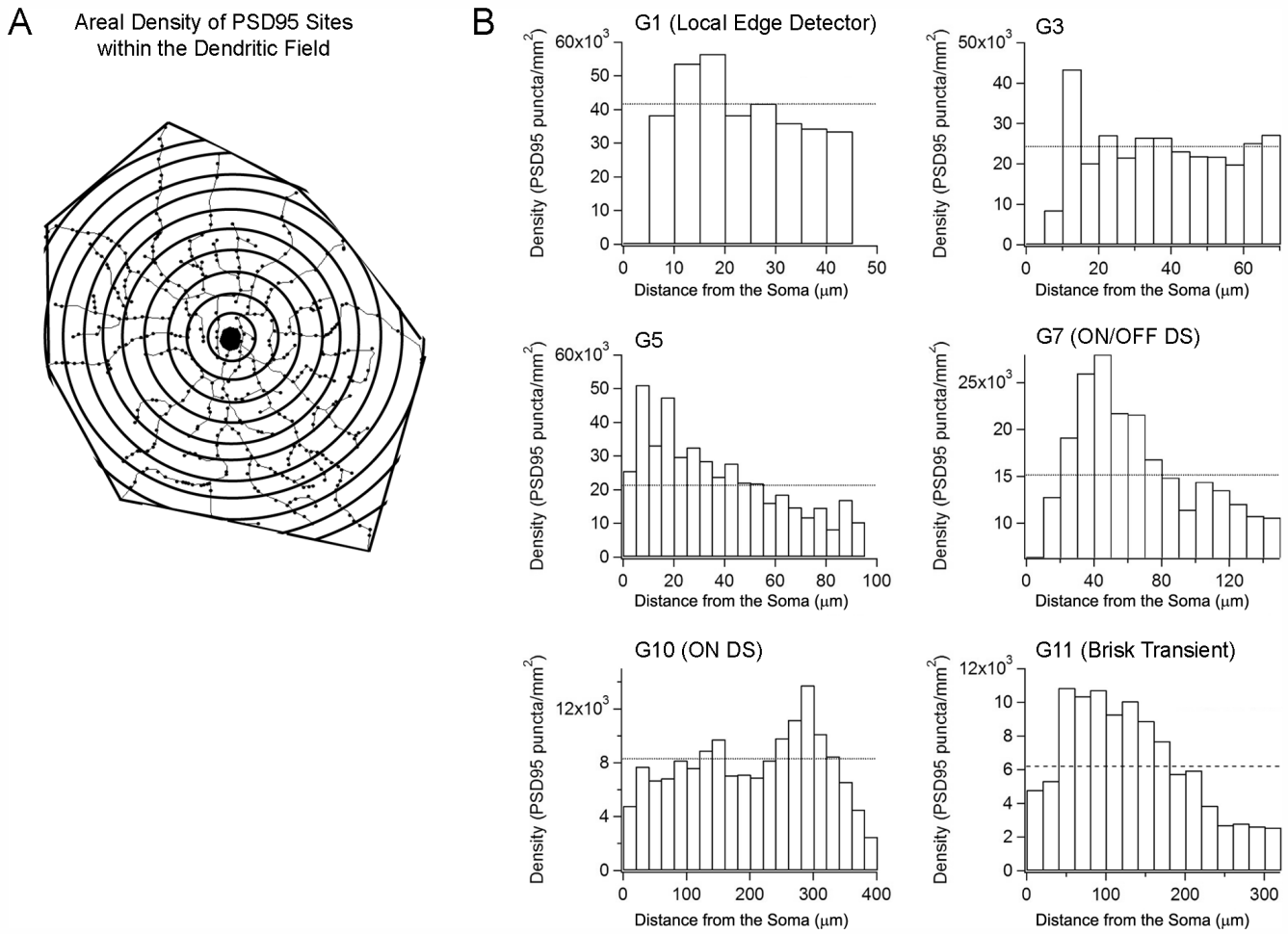

Figure 7. Two-dimensional distribution of PSD95 within dendritic field

(A) Bins were created in concentric zones centered upon the soma. The density of PSD95-GFP within each bin was calculated (puncta / μm^2). To avoid the distortion potentially created by the irregular profile of terminal dendrites, only concentric zones that were at least 80% contained within the convex hull were considered. **(B)** The histograms show the density of puncta within those bins as a function of distance from the soma. For all cells, there is a low density of PSD95 sites near the soma. This corresponds to the fact that few synapses are made upon the dendrites that connect the soma to the main stratified arbor of the cell. Four of the cell types show a peak of density at a location slightly displaced from the soma — in the full two-dimensional arbor this creates a ring-shaped peak of density. The one exception is an ON direction selective cell, which had a very asymmetric arbor (see Figure 4).

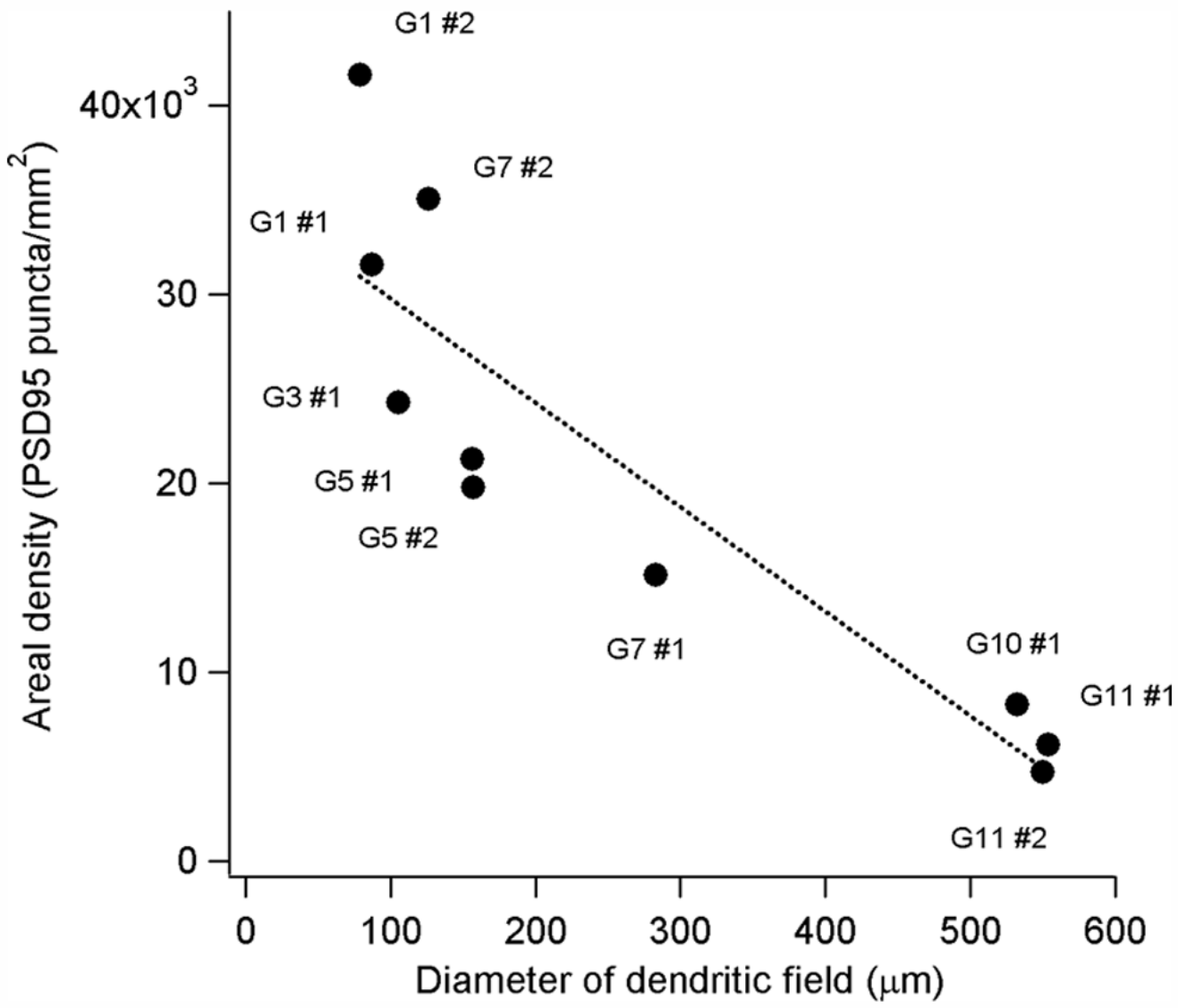

Figure 8. Relationship between dendritic field size and number of PSD95 sites

The graph shows the total number of PSD95 sites within the dendritic arbor (i.e. contained within the convex hull) divided by the area of the dendritic field. This represents the total number of PSD95 sites afferent to that cell. The dotted line shows a linear fit to the data (Pearson r = -0.89).

Table 1

The set of labeled cells chosen for analysis, with their PSD95 densities.

Type	Cell	Number of PSD95 Puncta	Dendritic field diameter (µm)	Total length of dendrites (µm)	puncta / linear µm	Mean interval (µm)	SD	SEM
G1 (Local edge detector)	#1	187	86.86	1034.80	0.18	5.72	4.81	0.37
	#2	204	78.98	831.46	0.25	4.75	3.69	0.26
G3	#1	316	104.91	1144.40	0.28	3.09	2.15	0.12
G5	#1	406	156.39	1678.70	0.24	4.47	2.91	0.14
	#2	381	156.63	2050.30	0.19	5.45	3.73	0.20
G7 (ON/OFF DS)	#1	1537	282.94	6707.30	0.23	4.65	4.94	0.13
	#2	565	126.16	2503.40	0.23	4.21	3.67	0.16
G10 (ON DS)	#1	1845	531.87	9625.80	0.19	5.27	4.48	0.10
G11 (Brisk transient)	#1	1492	553.41	8470.30	0.18	5.59	4.22	0.11
	#2	1121	549.37	7732.60	0.15	6.75	4.05	0.12